Surface solar irradiance estimation with low-cost fish-eye camera

Charlotte Gauchet, Philippe Blanc, Bella Espinar, Bruno Charbonnier, Dominique Demengel

Surface solar irradiance estimation with low-cost fish-eye camera

C. Gauchet[1,2], P. Blanc[1], B. Espinar[1], B. Charbonnier[2], D. Demengel[2]
[1] MINES ParisTech, CEP – Centre Energétique et Procédés, Sophia Antipolis, France, *philippe.blanc@mines-paristech.fr*
[2] EDF R&D, Chatou, France, *bruno.charbonnier@edf.fr*

***Abstract*—This communication deals with a prototype of a low-cost fish-eye camera developed by EDF R&D, meant to be an alternative for local and very short term solar forecasting to standard total sky imagers. The paper presents the results of a preliminary study demonstrating a very important pre-requisite for the use of fish-eye camera for solar forecasting purpose: the relationship between hemispheric sky images and the different components (global, diffuse and direct) of the surface solar irradiance (SSI). This study has been carried out with high quality "BSRN quality level" radiometric data and hemispheric sky images from a EDF R&D's test site on Reunion Island, in the Indian Ocean. This experimental study leads to very concluding and promising results on sub-hourly estimation of diffuse, direct and global SSI from sky images provided by the fish-eye camera.**

I. Nomenclature

BHI: Beam (or direct) horizontal irradiance (W/m^2)
BNI: Beam (or direct) normal irradiance (W/m^2)
BSRN: Baseline Surface Radiation Network
DHI: Diffuse horizontal irradiance (W/m^2)
EDF: Electricité de France
GHI: Global horizontal irradiance (W/m^2)
RGB: Red green blue image
SSI: Surface solar irradiance (W/m^2)
TSI: Total sky imager

II. Introduction

Local and very short term sub-hourly forecast of the electric production of solar power plants is useful for producers and grid operators to cope with solar radiation temporal variability, by helping them to efficiently schedule, dispatch and regulate electric power generation and demand.

Unfortunately, numerical weather prediction and state-of-art geostationary satellite-based forecast approaches are limited by their spatial and temporal resolution, too coarse for very short term forecast issues. In this context, forecast approaches based on ground based sky imager are very promising as it provides high temporal and spatial resolution hemispherical information of the cloud cover [3].

This communication deals with a prototype of a low-cost fish-eye camera developed by EDF R&D, meant to be an alternative for solar forecasting to standard total sky imagers (TSI). Indeed, these TSI include complex, not totally robust, and costly mechanical system of shadow band meant to prevent the direct solar irradiation from dazzling the digital camera.

In order to forecast solar radiation or solar electricity production with such fish-eye camera using cloud motion estimation, it is first needed to be able to determine a "radiation transfer function" between the hemispheric sky images and the concomitant corresponding global, direct and diffuse components of the surface solar irradiance (SSI).

This paper presents the results of an experimental study dealing with this relationship with radiometric data and concomitant hemispheric sky images from an EDF R&D's test site on Reunion Island, in the Indian Ocean. The different stages needed to establish this relationship are first described: geometric and radiometric calibrations, image segmentation (clear sky, bright and dark clouds, *circumsolar* area and solar disk) and determination of the regression models for estimation of the global, direct and diffuse surface solar irradiance from the hemispheric sky images. Then the performance of the fish-eye based estimation of the different components of the SSI is compared to on-ground high quality radiometric measurements.

III. Data Description from the test site

The test site set up by EDF R&D is located in the North-East part of Reunion Island, at the foot of the *Piton de la Fournaise* volcano.

The low-cost fish-eye camera has been installed in this site, providing, since November 2010, hemispheric sky images with 1200x1600 pixels, every 30 seconds. For this experimental study, approximately 89 000 sky images, from the month January 2011, have been considered.

This test site also includes a BSRN-quality-level pyranometer ground station with, in particular:

- a pyrheliometer mounted on a 2-axis sun-tracker for the BNI measurement;
- a pyranometer for the GHI measurement;
- a shadowband pyranometer for the DHI measurement;

Time series of GHI, DHI and DNI from this station have been used, with a temporal resolution of 10 seconds. Very strict quality checks have been applied to this solar radiation data, following quality check procedures described in [9].

The Fig. 1 shows an example of the RGB hemispheric sky image from the fish-eye camera for the day 2011/01/16 at 12:43:06 (UT+4). The figure also represents the daily time series of GHI, DHI and BNI for the corresponding day.

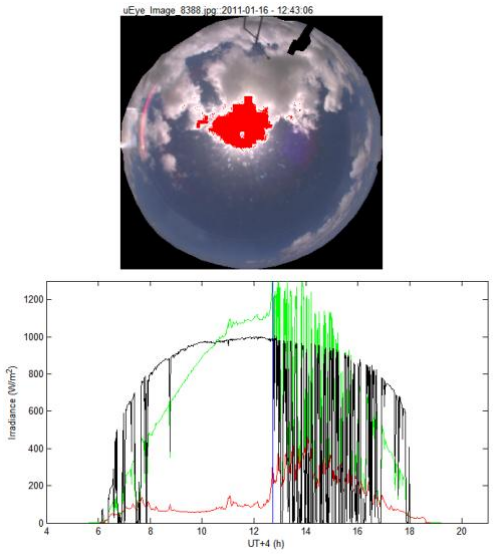

Fig. 1. Example of the hemispheric sky image for the day 2011/01/16 at 12:43:06 (UT+4) and the GHI (green), DHI (red) and BNI (black) measured for the corresponding day. Red pixels in the hemispheric sky image correspond to saturated pixels.

IV. Geometric Calibrations of the Fish Eye Camera

A. Intrinsic geometric calibration

The determination of a radiation transfer function between hemispheric sky images and concomitant SSI first requires being able to locate precisely the sun position in the hemispheric images and, inversely, to determine for each pixel, the corresponding topocentric spherical coordinates elevation and azimuth. The determination of this direct – *camera-to-world* – and inverse, *world-to-camera* – localization or transfer functions are also needed for the forecast processing, in particular to ease automatic image-based cloud motion estimation [6].

In order to assess this geometric localization function, we have first recourse to a technique – together to a Matlab® toolbox – meant to calibrate omnidirectional camera [10]. This technique only requires some images of a planar chessboard target with different orientations. The Fig. 2 depicts the four images of A0-format planar chessboard target approximately corresponding to the four cardinal points. As both, position and orientation, of this planar target for these four images were not intend to be accurately positioned at the four cardinal points, the calibration technique was "only" meant to determine the intrinsic geometric calibration of the camera, thus determining the localization function with respect to a local frame peculiar to the fish-eye camera.

B. Extrinsic geometric calibration

Euler angles of this intrinsic local frame with respect to the North, West, Up coordinate system remains to be determined to get the final localization function: this corresponds to the extrinsic calibration. This extrinsic calibration made use of a specific optimization iterative procedure with respect to these Euler angles to minimize the mean square error between:

- The sun's pixel positions automatically detected by the camera on a large subset of sky images under clear sky conditions ;
- The corresponding theoretical sun's pixel positions determined by the inverse localization function whose extrinsic parameters are under optimization. Accurate topocentric sun positions are provided by the fast solar geometry algorithm presented in [1].

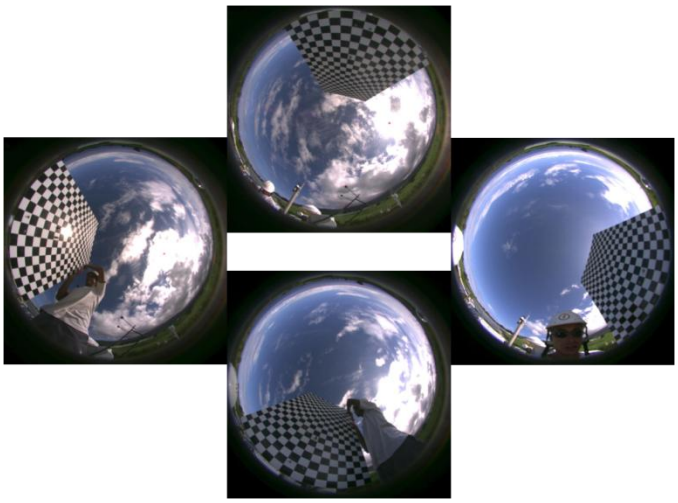

Fig. 2. Images from the fish-eye camera of the planar A0 chessboard target at approximately the four cardinal points.

V. Image Segmentation of the Sky Images

A. Principle of the pixel-wise segmentation

The aim of the pixel-wise segmentation is to "simplify" hemispheric RGB sky images into segmented images with five classes relevant for the determination of the radiation transfer function:

- Class C_1: clear sky;
- Class C_2: bright cloud;
- Class C_3: dark cloud;
- Class C_4: non-occulted pixels in the solar disk;
- Class C_5: non-occulted pixels in the circumsolar disk;

Considering the practical constraints of a real-time and onboard forecast processing based on the fish-eye camera, the segmentation algorithm should be as "simple" as possible. Standard segmentation algorithms for hemispheric sky images (*cf.* [2], [4] or [5]) are usually simply based on threshold applied on the R/G ratio.

In this study we have developed a new segmentation approach: for the classes C_1, C_2 and C_3 the segmentation are based on thresholds on the luminance channel L = 0.2126 R + 0.7152 G + 0.0722 B and on the difference B-R. Different thresholds are defined with respect to specific zones: "Extended circumsolar disk", "sky horizon" and "main zone" as depicted by the Fig. 3. For the classes C_4 and C_5, the segmentation is based on a pixel saturation test applied on the corresponding solar and circumsolar zones.

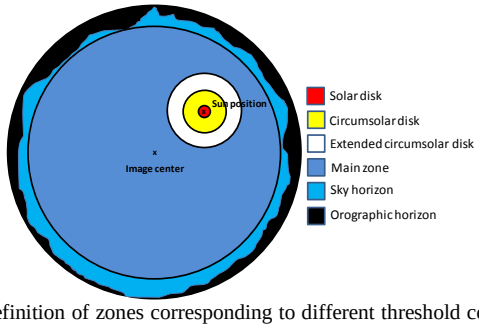

Fig. 3. Definition of zones corresponding to different threshold conditions for the proposed segmentation.

B. *Results and validation*

The Fig. 4 shows an example of the segmentation result.

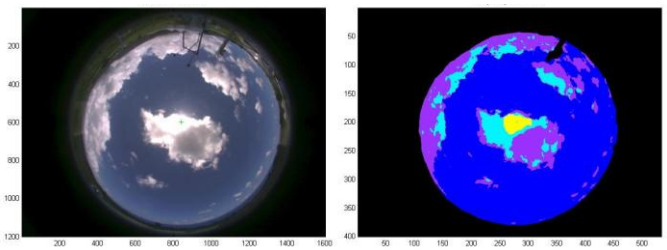

Fig. 4. Example of the segmentation result (right) of the hemispheric sky image (left) at the day 2011/01/16 at 12:43:06 (UT+4).

Segmentation validation has been carried out on a subset of representative sky images for which a total of approximately 1000 pixels has been "manually" classified by human operators. Among these manually classified pixels, 86 % has been correctly classified by the proposed segmentation algorithm into the "clear sky", "bright clouds" and "dark clouds" classes; more than 92 % has been correctly classified if no distinction between the two cloud classes is considered.

VI. ESTIMATION OF THE SURFACE SOLAR IRRADIANCE

A. *Determination of the radiation transfer functions*

Let note $\gamma(x,y)$ and $\phi(x,y)$ the two components – resp. topocentric elevation and azimuth angles – of the direct localization function for the pixel (x,y). Each sky element corresponding to this pixel contributes to the horizontal irradiance with a weighting factor W_H:

$$W_H(x,y) = \frac{1}{\pi} \sum_{\gamma(x,y)>0} \cos\gamma(x,y) \sin\gamma(x,y) J(x,y) \qquad (1)$$

$$\text{where } J(x,y) = \left| \frac{\partial\gamma}{\partial x}(x,y) \frac{\partial\phi}{\partial y}(x,y) - \frac{\partial\gamma}{\partial y}(x,y) \frac{\partial\phi}{\partial x}(x,y) \right|$$

The four components of the gradient of the direct localization function are obtained by a finite difference method.

The radiation transfer model for horizontal irradiances (global, direct and diffuse) is in the form:

$$\left(\alpha_0 + \sum_{k=1}^{5} \alpha_k \left(\sum_{(x,y)\in C_k} W_H(x,y) \right) \right) I_{CLS} \qquad (2)$$

I_{CLS} is the corresponding horizontal irradiance under clear sky condition based on the ESRA model [8] with Linke turbidity estimation at the test site obtained from www.soda-is.com with a methodology described in [7]. Note that the direct normal irradiance is obtained from the direct horizontal irradiance divided by the sinus of the sun's elevation angle.

The six coefficients $\{\alpha_k\}$ for each irradiance component are determined by a linear regression, using the concomitant corresponding measured horizontal irradiance.

B. *Results*

The Table 1 presents the results of the comparison between the different components of irradiance estimated with the radiation transfer function from the fish-eye camera images and the corresponding values from the radiometric ground station. The different irradiances have been aggregated with a sampling and an integration period of 5 minutes. Irradiance data corresponding to a sun elevation angle below 10° have been filtered out from the comparisons.

The Fig. 5 shows the differences between the calculated values of each of the solar radiation components from the fish-eye camera images with respect to the measured values from the ground station for the day of 2011/01/05.

	MREF (W/m^2)	MBE (%)	RMSE (%)	CC
GHI	566	0 %	17 %	0.959
DHI	223	-6 %	32 %	0.915
BHI	450	1 %	22 %	0.950
BNI	588	1 %	21 %	0.963

Table 1. Comparison between estimated and measured 5-min GHI, DHI, BHI and BNI irradiances for the month January 2011 and sun elevation angle greater than 10°. MREF: Mean value of the measured time series of irradiance (W/m^2). MBE: Mean Bias Error of the estimation relative to MREF (%). RMSE: Root Mean Square Error of the estimation relative to MREF (%). CC: Correlation Coefficient.

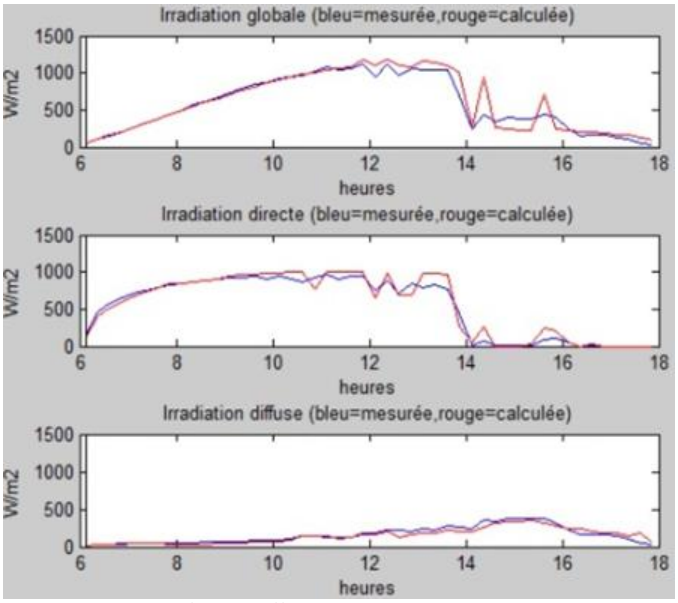

Fig. 5. Example of the differences between the measured radiation components (blue) and the estimated values from the fish-eye camera images (red) for the three solar radiation components (GHI on the top, BNI in the middle and DHI in the bottom) for the day 2011/01/06.

The Table 2 presents comparisons with irradiance data aggregated with a sampling and an integration period of 1 hour.

	MREF (W/m^2)	MBE (%)	RMSE (%)	CC
GHI	587	0 %	8 %	0.986
DHI	235	-4 %	23 %	0.943
BHI	402	1 %	13 %	0.987
BNI	519	1 %	13 %	0.984

Table 2. Comparison between estimated and measured 1-hour GHI, DHI, BHI and BNI irradiances for the month January 2011 and sun elevation angle greater than 10°.

VII. Conclusion and perspectives

This communication presents an experimental study dealing with SSI estimation with low-cost fish-eye camera as a pre-requisite for very short term SSI forecasting purpose.

This SSI estimation requires first a geometric calibration of the fish-eye camera in order to establish the direct and inverse localization functions. The different SSI components are then estimated by the use of specific radiation transfer functions established by linear regression and applied to sky images segmented into five classes: clear sky, bright and dark clouds and occulted pixels on the circumsolar and solar disks.

Comparisons with concomitant high quality radiometric ground data shows very good performances of the sub-hourly and hourly estimations not only of the GHI but also the DHI, the BHI and the BNI. This fact is a specificity and an advantage of the fish-eye camera compared to standard TSI that are equipped with a mechanical system of shadow band meant to prevent the direct solar radiation from dazzling the digital camera: for TSI no information are therefore intrinsically available in the neighborhood of the sun position.

The assessment of quality of the fish-eye based SSI estimation has been carried out with a set of sky images and radiation data limited to one month on one test site. Nevertheless, the very high temporal and spatial variability of the cloud coverage during the month of January 2011 for this test site allows us to consider these good performances as very promising.

The next development of the research activity related to this low-cost fish-eye camera will focus on the very short term forecast of the different SSI components. This forecast algorithm is planned to be based on cloud motion estimation algorithm in connection with the segmentation algorithm and the radiation transfer functions presented in this communication.

VIII. References

[1] P. Blanc, L. Wald, "A library for computing the relative position of the Sun and the Earth", ENDORSE FP7 project (Grant Agreement no 262892), Tech. Rep. D3.1. Available: http://www.endorse-fp7.eu/sites/www.endorse-fp7.eu/files/docs/endorse_d3.1v1.1.pdf.

[2] J. Calbo, J. Sabburg, "Feature Extraction from Whole-Sky Ground-Based Images for Cloud-Type Recognition", *Atmospheric and Oceanic Technology*, pp. 159–169, 2004.

[3] C. W. Chow, B. Urquhart, M. Lave, A. Dominguez, J. Kleissl, J. Shields and B. Washom, "Intra-hour forecasting with a total sky imager at the UC San Diego solar energy testbed", *Solar Energy*, vol. 85, no. 11, pp. 2881-2893, Nov. 2011.

[4] A. Heinle, A. Macke, A. Srivastav, "Automatic cloud classification of whole sky images", *Atmospheric Measurement Techniques*, vol. 25, pp. 3–14, Jan. 2008.

[5] C.N. Long, J.M. Sabburg, J. Calbo, D. Pagès, "Retrieving Cloud Characteristics from Ground-Based Daytime Color All-Sky Images", *Atmospheric and Oceanic Technology*, vol. 23, pp. 633–652, May 2006.

[6] G. D. Modica, G. D., R. d'Entremont, E. Mlawer, and E. Gustafson, "Short-range solar radiation forecasts in support of smart grid technology", in *Proc. 2010 1st Conf. on Weather, Climate, and the New Energy Economy*, Atlanta, GA, Amer. Meteor. Soc., J12.3.

[7] J. Remund, L. Wald, M. Lefevre, T. Ranchin, J. Page, "Worldwide Linke turbidity information". In *Proc. 2003 of ISES Solar World Congress*, 16-19 June 2003, Göteborg, Sweden.

[8] C. Rigollier and O. Bauer, "On the clear sky model of the ESRA — European Solar Radiation Atlas — with respect to the HELIOSAT method", *Solar energy*, vol. 68, no. 1, pp. 33-48, 2000.

[9] A. Roesch, M. Wild, A. Ohmura, E. G. Dutton, C. N. Long, and T. Zhang, "Assessment of BSRN radiation records for the computation of monthly means", *Atmospheric Measurement Techniques*, vol. 4, no. 2, pp. 339-354, Feb. 2011.

[10] D. Scaramuzza, A. Martinelli, R. Siegwart, "A toolbox for easily calibrating omnidirectional cameras", in *Proc. 2006 IEEE/RSJ International Conference on Intelligent Robots and Systems*, pp. 5695-5701.